This article has been accepted for publication in a future issue of this journal, but has not been fully edited. Content may change prior to final publication. Citation information: DOI 10.1109/LCOMM.2017.2765307, IEEE Communications Letters

Theoretical Analysis of 3D Channel Spatial Correlation and Capacity

Yawei Yu*, Jianhua Zhang*, Peter J. Smith†, Pawel A. Dmochowski†

***Abstract*—In this letter, an approximate closed-form expression for 3D channel spatial correlation (SC) is derived, given cross-polarized rectangular arrays and standards based antenna radiation patterns. Furthermore, we evaluate the impact of 3D SC on system performance and derive the capacity relationship between 2D and 3D channels. As expected, the 3D channel is characterized by lower SC and higher channel capacity than its 2D counterpart by taking advantage of the additional degrees of freedom in the elevation domain, where 3D antenna arrays and 3D channel propagation are considered.**

***Index Terms*—3D Channel; Spatial Correlation; Channel Capacity.**

I. Introduction

To meet the high capacity requirements in 5G communication [1], 3D MIMO, which makes use of the additional degrees of freedom in elevation domain to enable strategies such as sector beamforming and cell interference mitigation [2], has been investigated. Preliminary results on 3D channel modeling have been reported [3], a large effort is made to get accurate 3D channel models that support the elevation domain. Recent field measurements in an outdoor-to-indoor scenario demonstrate a large channel capacity gap between 2D and 3D channel models [4]. As demonstrated by the analysis in [5], this is attributed in a great part to the reduction in the antenna spatial correlation (SC) with the increase in vertical antenna spacing (VAS) and elevation angle spread (EAS). Under different angle spreads and antenna spacings, closed-form expressions of 3D SC for various antenna arrays were investigated in [6]. However, [6] did not consider practical antenna radiation patterns due to the lack of standardized 3D models even though system performance is closely related to antenna radiation efficiencies [7]. Based on the Fourier coefficients of antenna radiation patterns, a general closed-form expression for 3D SC for a uniform linear antenna array was proposed in [8].

In this letter, we extend these prior works on 3D SC and make the following contributions:

- Given a cross-polarized uniform rectangular array (URA) and standards based antenna radiation patterns [9], we derive, and evaluate the accuracy of, an approximate closed-form expression for 3D SC.
- Numerical simulation results demonstrate that when VAS $= 0.5\lambda$, 3D SC will be lowered to 0.60, 0.52, 0.35 for EAS $= 30^o$, 60^o and 90^o, respectively.
- We derive bounds for 3D channel capacity, which show a clear relationship between 2D and 3D channel capacity. A large channel capacity increase (>38% at EAS=10^o) from 2D to 3D channels has been observed, and this gap is further enhanced with larger EAS.
- We conclude that the 3D channel will achieve lower SC and higher channel capacity than its 2D counterpart due to the additional freedom in the elevation domain, which highlights the importance of 3D channel utilization.

The remainder of this letter is outlined as follows: Section II gives the closed-form expression for 3D SC, followed by the channel capacity relationship between 2D and 3D models in Section III. Then, conclusions are drawn in Section V.

Notation: $U(a,b)$, $VM(\mu_0,\kappa)$, $\mathcal{CN}(\mu_1,\sigma^2)$, $J_0(\cdot)/I_0(\cdot)$, $\odot$ denote the uniform distribution within (a,b), Von-Mises distribution with mean value μ_0 and dispersion factor κ, complex Gaussian distribution with mean value μ_1 and standard derivation σ, the zeroth order modified Bessel function of the first/second kind, the Hadamard product, respectively.

II. Closed Form Expression for 3D SC

Considering the 3D channel model in the most recent standard [9] and assuming the elevation angle θ and azimuth angle ϕ are independent variables, the 3D SC between element m and m' of the URA in Fig. 1 is given by [5]

$$R^{\text{3D}}_{mm'} = \begin{cases} \dfrac{\mathbb{E}\{A_V(\theta)A_H(\phi)e^{-j2\pi \boldsymbol{r}^T(\boldsymbol{d}_m-\boldsymbol{d}_{m'})}\}}{\mathbb{E}\{A_V(\theta)\}\mathbb{E}\{A_H(\phi)\}} & \text{for } \xi_m=\xi_{m'}, \\ 0 & \text{for } |\xi_m-\xi_{m'}|=\pi/2, \end{cases} \quad (1)$$

where

- $A_V(\theta)$ and $A_H(\phi)$ denote the antenna radiation patterns in the elevation and azimuth domain, respectively, where

$$A_V(\theta)\text{ dB} = -\min\left[12\left(\frac{\theta-90^o}{\theta_{\text{3dB}}}\right)^2, SLA_v\right], \quad (2)$$
$$\theta_{\text{3dB}}=65^o, \quad SLA_v=30\text{ dB},$$

$$A_H(\phi)\text{ dB} = -\min\left[12\left(\frac{\phi}{\phi_{\text{3dB}}}\right)^2, A_m\right], \quad (3)$$
$$\phi_{\text{3dB}}=65^o, \quad A_m=30\text{ dB}.$$

- $\boldsymbol{r}$ denotes the spherical unit vector of the transmitted (or received) path

$$\boldsymbol{r}=[\sin(\theta)\cos(\phi),\sin(\theta)\sin(\phi),\cos(\theta)]^T. \quad (4)$$

- $\boldsymbol{d}_m$ and $\boldsymbol{d}_{m'}$ denote the location vectors of element m and m', respectively, given by

$$\boldsymbol{d}_m=(dx_m,dy_m,dz_m)^T, \boldsymbol{d}_{m'}=(dx_{m'},dy_{m'},dz_{m'})^T. \quad (5)$$

- ξ_m and $\xi_{m'}$ denote the polarization slant angles of the antenna m and m', respectively.

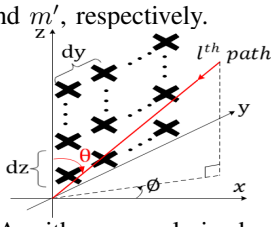

Fig. 1: URA with cross-polarized antenna pairs

*Yawei Yu and Jianhua Zhang are with Beijing University of Posts and Telecommunications, Beijing, China (emails: yyw@bupt.edu.cn; jhzhang@bupt.edu.cn).

†Peter J. Smith and Pawel A. Dmochowski are with Victoria University of Wellington, New Zealand (emails: peter.smith@ecs.vuw.ac.nz; pawel.dmochowski@ecs.vuw.ac.nz).

The research is supported by National Natural Science Foundation of China and project name is 'Theoretical Modeling and Experiment Research of Propagation Channel' with NO. 61322110.

This article has been accepted for publication in a future issue of this journal, but has not been fully edited. Content may change prior to final publication. Citation information: DOI 10.1109/LCOMM.2017.2765307, IEEE Communications Letters

Since $R^{3D}_{mm'}$ is assumed to be zero for cross-polarized antennas with $|\xi_m - \xi_{m'}| = \frac{\pi}{2}$ [5], we focus on $R^{3D}_{m,m'}$ for co-polarized antennas where $\xi_m = \xi_{m'}$ and derive its closed-form expression.

Lemma 1: Assuming $\phi \sim U(-\pi, \pi)$ and $\theta \sim VM(\frac{\pi}{2}, \kappa)$ [8], the approximate closed-form expression for $R^{3D}_{mm'}$ is given in (6) (the next page), where

- d_{xy} is the distance between elements m, m' in the $x-y$ plane
$$d_{xy} = \sqrt{d_x^2 + d_y^2}, \tag{7}$$
where d_x and d_y denote the spacing between elements m and m' along x axis and y axis, respectively. Here we ignore the index m and m' for simplicity.
- Δ is related to d_x and d_y by $\Delta = \tan^{-1}(d_y/d_x)$.
- $\{a_n, n = 0, 1, 2, ..., N\}$ are the Fourier series coefficients of $A_H(x)$ given by
$$\begin{aligned} a_0 &= \frac{1}{2\pi}\int_{-\pi}^{\pi} A_H(x)dx, \\ a_n &= \frac{1}{\pi}\int_{-\pi}^{\pi} A_H(x)\cos(nx)dx. \end{aligned} \tag{8}$$
- A series expansion of $e^{-j2\pi dz\cos\theta}$ is given by
$$e^{-j2\pi dz\cos\theta} = J_0(-2\pi dz) + 2\sum_{r=1}^{R} j^r J_r(-2\pi d_z)\cos(r\theta). \tag{9}$$
- N_{1r}, N_{2r} are given by
$$N_{1r} = (n-l)/2,\ N_{2r} = (n+l)/2. \tag{10}$$
- The probability density function, $f(\theta)$, for a Von-Mises distribution is given by
$$f(\theta) = e^{\kappa\sin\theta}/(2\pi I_0(\kappa)) = c_\kappa f_1(\theta), \tag{11}$$
where $f_1(\theta) = e^{\kappa\sin\theta}/e^{\kappa}$ and $c_\kappa = e^{\kappa}/(2\pi I_0(\kappa))$.
- k_l $(l = 0, 1, 2, ...)$ denote the expansion coefficients of $\sin(\theta)^{2L}$ in (23) and are given by
$$k_0 = \tfrac{1}{2^{2L}}\binom{2L}{L}, k_l = \tfrac{1}{2^{2L}}(-1)^l 2\binom{2L}{L-l} \text{ for } l > 0. \tag{12}$$

Proof: See Appendix V-A.

Note that, $A_V(\theta)f_1(\theta) \approx \sin(\theta)^{2L}$ is the only approximation used in deriving (6) and can be used under different elevation angle distributions such as Von-Mises, Laplacian, Wrapped Gaussian distributions, etc. For the narrower Von-Mises distributions (larger κ), a larger value of L is needed. For example, when $\kappa = 4, 2, 0$ (EAS values are $30^o, 60^o, 90^o$), we approximate the term $A_V(\theta)f_1(\theta)$ by $\sin(\theta)^8$, $\sin(\theta)^6$ and $\sin(\theta)^4$, respectively, and the approximation accuracy is validated in Fig. 2.

In Fig. 3, we show the variation of $R^{3D}_{m,m'}$ with d_y and d_z under different EASs (different κ). As $a_n \to 0$ rapidly as n increases, using only a few terms (say $N = 5$) gives a high accuracy. Similarly, a small number of the expansion terms in (9) is used (say $R = 4$). It can be seen that larger antenna spacing in the y or z axis greatly reduces the SC. When d_y or d_z reaches 0.5λ, the SC is lowered to 0.5 approximately. Larger EAS will lower the SC in Fig. 3(b) while $R^{3D}_{mm'}$ for different EASs in Fig. 3(a) shows minor differences when $d_z = 0$. For all the above cases, the approximate 3D SC in (6), $R^{3D,app}_{mm'}$, fits very well with the true value $R^{3D}_{mm'}$. Thus, the derivation of (6) provides a general method to calculate the closed-form expression for 3D SC with high approximation accuracy.

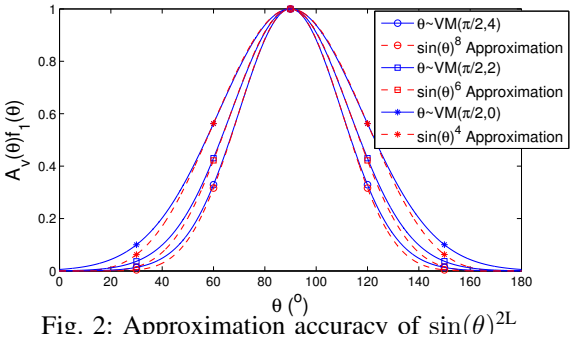

Fig. 2: Approximation accuracy of $\sin(\theta)^{2L}$

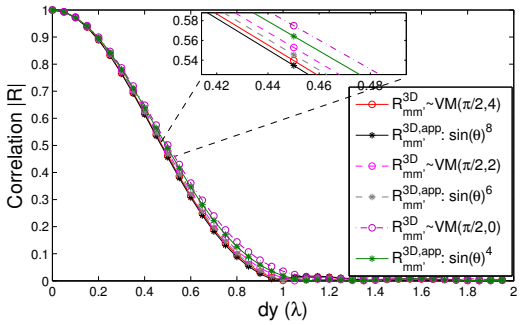

(a) $R^{3D}_{mm'}(0, dy, 0)$ with d_y

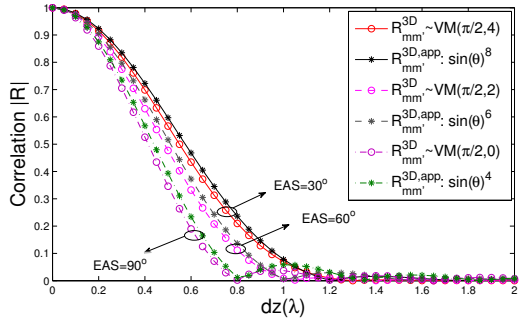

(b) $R^{3D}_{mm'}(0, 0, dz)$ with d_z

Fig. 3: Variation of $R^{3D}_{mm'}(d_x, d_y, d_z)$ with d_y and d_z

III. Channel Capacity

The above 3D SC is given for a specific cluster-based channel model (CBCM), where the capacity gap between 2D and 3D channel models is difficult to derive due to the complicated components. However, results in [10] show a close similarity between eigenvalues of the CBCM and Kronecker channel model. This implies that we could apply the calculated SC to a Kronecker channel model in the ergodic capacity analysis, aiming to obtain the capacity relationship between 2D and 3D channels. Assuming a simple Rayleigh fading channel
$$\mathbf{H} = \mathbf{R}_{\text{Rx}}^{1/2}\mathbf{G}\mathbf{R}_{\text{Tx}}^{1/2}, \tag{13}$$
where $\mathbf{G} \in \mathcal{C}^{Q\times M}$ has $\mathcal{CN}(0,1)$ entries and M and Q denote the Tx and Rx antenna numbers, respectively. The capacity is computed as [11]
$$C = \mathbb{E}\left\{\log_2\det\left(\mathbf{I} + \tfrac{\text{SNR}}{\beta M}\mathbf{H}^{\text{H}}\mathbf{H}\right)\right\}, \tag{14}$$
where β is the normalization factor, thus $\mathbb{E}\left\{\frac{1}{\beta}||\mathbf{H}||_{\text{F}}^2\right\} = MQ$.

This article has been accepted for publication in a future issue of this journal, but has not been fully edited. Content may change prior to final publication. Citation information: DOI 10.1109/LCOMM.2017.2765307, IEEE Communications Letters

$$R^{\text{3D}}_{m,m'} \approx R^{\text{3D,app}}_{mm'} = \frac{1}{\pi a_0 k_0}\sum_{n=0}^{N} a_n(-j)^n\cos(n\Delta)\left\{\sum_{l=0}^{L} k_l\pi\left[J_0(-2\pi d_z)J_{\frac{n}{2}-l}(\pi d_{xy})J_{\frac{n}{2}+l}(\pi d_{xy}) + \sum_{r=1}^{R} j^r J_r(-2\pi d_z)\left(\cos(N_{1r}\pi)J_{\frac{n}{2}-N_{1r}}(\pi d_{xy})J_{\frac{n}{2}+N_{1r}}(\pi d_{xy}) + \cos(N_{2r}\pi)J_{\frac{n}{2}-N_{2r}}(\pi d_{xy})J_{\frac{n}{2}+N_{2r}}(\pi d_{xy})\right)\right]\right\}, \tag{6}$$

Lemma 2: 2D capacity, C_{2D}, and the bounding 3D capacity, C^B_{3D}, are given below:

$$C_{\text{2D}} = \mathbb{E}\left\{\log_2\det\left(\mathbf{I} + \frac{\text{SNR}}{\beta M}\mathbf{G}^H\mathbf{R}^{\text{2D}}_{\text{Rx}}\mathbf{G}\mathbf{R}^{\text{2D}}_{\text{Tx}}\right)\right\}, \tag{15}$$

$$C^B_{\text{3D}}(\rho) = \mathbb{E}\left\{\log_2\det\left(\mathbf{I} + \frac{\text{SNR}}{\beta M}\left(\rho^2\mathbf{G}^H\mathbf{R}^{\text{2D}}_{\text{Rx}}\mathbf{G}\mathbf{R}^{\text{2D}}_{\text{Tx}} + \rho(1-\rho)\mathbf{R}_{\text{mix}} + (1-\rho)^2\mathbf{R}_{\text{i.i.d}}\right)\right)\right\},\ 0\le\rho\le 1, \tag{16}$$

where $\mathbf{R}_{\text{mix}} = \mathbf{G}^H\mathbf{I}_{\text{Rx}}\mathbf{G}\mathbf{R}^{\text{2D}}_{\text{Tx}} + \mathbf{G}^H\mathbf{R}^{\text{2D}}_{\text{Rx}}\mathbf{G}\mathbf{I}_{\text{Tx}}$ is a mixed component when $\mathbf{R}_{\text{Rx}} = \mathbf{I}_{\text{Rx}}$ or $\mathbf{R}_{\text{Tx}} = \mathbf{I}_{\text{Tx}}$, $\mathbf{R}_{\text{i.i.d}} = \mathbf{G}^H\mathbf{I}_{\text{Rx}}\mathbf{G}\mathbf{I}_{\text{Tx}}$ denotes the i.i.d correlation component when both $\mathbf{R}_{\text{Rx}} = \mathbf{I}_{\text{Rx}}$ and $\mathbf{R}_{\text{Tx}} = \mathbf{I}_{\text{Tx}}$. Here, $\mathbf{I}_{\text{Tx}}$ and $\mathbf{I}_{\text{Rx}}$ denote the unit matrix in a dimension of $M\times M$ and $Q\times Q$, respectively.

Proof: See Appendix V-B

Lemma 3: Picking different values of ρ in (16), we can obtain the loose and tight bounds for 3D channel capacity:

(1) loose bound: $C_{\text{2D}} = C^B_{\text{3D}}(1) \le C_{\text{3D}} \le C^B_{\text{3D}}(0) \triangleq C_{\text{i.i.d}}$.

(2) tight bound: $C^{low}_{\text{3D}} \triangleq C^B_{\text{3D}}(\rho_0) \le C_{\text{3D}} \le C^B_{\text{3D}}(\rho_1) \triangleq C^{up}_{\text{3D}}$, with $\rho_0 = 1-2\pi^2 d^2_{z,0}\varepsilon^2/3$, $\rho_1 = 1-2\pi^2 d^2_{z,1}\varepsilon^2/3$, where ε denotes the EAS, $d_{z,0}$ and $d_{z,1}$ denote the minimum and maximum vertical spacing between antenna pairs, respectively.

Proof: See Appendix V-C

As we can see, $C_{\text{2D}} \le C^{low}_{\text{3D}} \le C_{\text{3D}} \le C^{up}_{\text{3D}} \le C_{\text{i.i.d}}$. In Fig. 4, we examine the capacity bounds in Lemma 3 for a 32×8 MIMO system (4×4 cross-polarized pairs at the Tx, 2×2 cross-polarized pairs at the Rx) with $d_y = 0.5\lambda$, $d_z = 0.5\lambda$, $d_{z,0} = d_z$, $d_{z,1} = 3d_z$ under different EASs. A large capacity gap between C_{3D} and C_{2D} can be observed (38.4% at SNR=25 dB, EAS=10^o) and larger EAS values will expand the gap. The derived tight bounds fit well with C_{3D} for both EAS=10^o and 20^o. By increasing the EAS, C_{3D} tends to $C_{\text{i.i.d}}$.

IV. Conclusion

In this letter, we further investigate the superiority of the 3D channel over its conventional 2D counterpart in terms of SC and channel capacity. Given the cross-polarized URA and the standards based radiation patterns, an approximate closed-form expression for 3D SC has been derived with high approximation accuracy (see Fig. 2). By using the elevation domain (VAS and EAS), the 3D channel has a much lower SC than the 2D counterpart (see Fig. 3), and a higher channel capacity is expected (see Fig. 4) with capacity bounds being derived in Lemma 3. Collectively, these analyses highlight the significance of the elevation domain and indicate a promising future for 3D channel utilization.

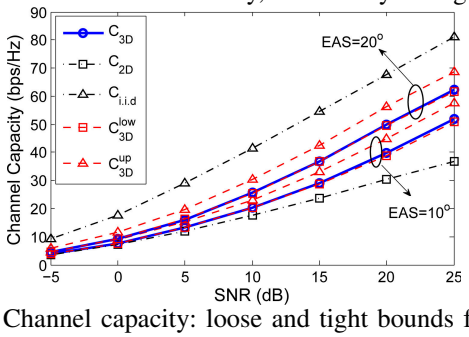

Fig. 4: Channel capacity: loose and tight bounds for C_{3D}

V. Appendix

A. Proof of Lemma 1

Assuming a uniform distribution for the azimuth angle, (1) can be rewritten as

$$R^{\text{3D}}_{mm'} = R^{\text{3D,Num}}_{mm'}/R^{\text{3D,Den}}_{mm'}, \tag{17}$$

where $R^{\text{3D,Num}}_{mm'}$ is given in (18). Then, (19) is obtained via the Fourier series expansion, $A_H(\Phi) = \sum_{n=0}^{N} a_n\cos(n\Phi)$, and the transform $d_x\sin\theta\cos\phi + d_y\sin\theta\sin\phi = d_{xy}\sin\theta\cos(\phi-\Delta)$. The decomposition $\cos(n\Phi) = \cos(n(\Phi-\Delta))\cos(n\Delta) + \sin(n(\Phi-\Delta))\sin(n\Delta)$ and integration of the azimuth angle over $[-\pi,\pi]$ in (20) gives (21), and (22) is obtained by (9). Using the the approximation $A_V(\theta)f_1(\theta) \approx \sin(\theta)^{2\text{L}}$ and the expansion of $\sin(\theta)^{2L}$ [12, (1.320.1)] where

$$\sin(\theta)^{2L} = \textstyle\sum_{l=0}^{L} k_l\cos(2l\theta), \tag{23}$$

with k_l defined in (12), we get (24). Further simplifications of (24) leads to (25), then (26) is based on [12, (6.681.9)]. Meanwhile, $R^{\text{3D,Den}}_{mm'}$ in (17) is given by

$$\begin{aligned} R^{\text{3D,Den}}_{mm'} &= \int_0^{\pi} A_V(\theta)f(\theta)d\theta\int_{-\pi}^{\pi} 10^{-1.2\left(\frac{\phi}{\phi_{\text{3dB}}}\right)^2}\frac{1}{2\pi}d\phi \\ &= \int_0^{\pi} c_\kappa A_V(\theta)f_1(\theta)d\theta\int_{-\pi}^{\pi}\sum_{n=0}^{N} a_n\cos(n\phi)\frac{1}{2\pi}d\phi \\ &= a_0c_\kappa\int_0^{\pi} A_V(\theta)f_1(\theta)d\theta \approx a_0c_\kappa\int_0^{\pi}\sin(\theta)^{2L}d\theta \\ &= a_0c_\kappa\int_0^{\pi}\sum_{l=0}^{L}\kappa_l\cos(2l\theta)d\theta = \pi a_0k_0c_\kappa. \end{aligned} \tag{27}$$

Substituting (26) and (27) into (17) gives the desired result of (6) in Lemma 1.

B. Proof of Lemma 2

Substituting (13) into (14), we have $C_{\text{2D}} =$

$$\begin{aligned} &\mathbb{E}\left\{\log_2\det\left(\mathbf{I} + \frac{\text{SNR}}{\beta M}(\mathbf{R}^{\text{2D}}_{\text{Tx}})^{\frac{1}{2},H}\mathbf{G}^H(\mathbf{R}^{\text{2D}}_{\text{Rx}})^{\frac{1}{2},H}(\mathbf{R}^{\text{2D}}_{\text{Rx}})^{\frac{1}{2}}\mathbf{G}(\mathbf{R}^{\text{2D}}_{\text{Tx}})^{\frac{1}{2}}\right)\right\} \\ &= \mathbb{E}\left\{\log_2\det\left(\mathbf{I} + \frac{\text{SNR}}{\beta M}(\mathbf{R}^{\text{2D}}_{\text{Tx}})^{\frac{1}{2},H}\mathbf{G}^H\mathbf{R}^{\text{2D}}_{\text{Rx}}\mathbf{G}(\mathbf{R}^{\text{2D}}_{\text{Tx}})^{\frac{1}{2}}\right)\right\}, \end{aligned} \tag{28}$$

further simplifications of (28) give that [13, Corollary 18.1.2]

$$\begin{aligned} C_{\text{2D}} &= \mathbb{E}\left\{\log_2\det\left(\mathbf{I} + \frac{\text{SNR}}{\beta M}\mathbf{G}^H\mathbf{R}^{\text{2D}}_{\text{Rx}}\mathbf{G}(\mathbf{R}^{\text{2D}}_{\text{Tx}})^{\frac{1}{2}}(\mathbf{R}^{\text{2D}}_{\text{Tx}})^{\frac{1}{2},H}\right)\right\} \\ &= \mathbb{E}\left\{\log_2\det\left(\mathbf{I} + \frac{\text{SNR}}{\beta M}\mathbf{G}^H\mathbf{R}^{\text{2D}}_{\text{Rx}}\mathbf{G}\mathbf{R}^{\text{2D}}_{\text{Tx}}\right)\right\}. \end{aligned} \tag{29}$$

Similarly, we have

$$C_{\text{3D}} = \mathbb{E}\left\{\log_2\det\left(\mathbf{I} + \frac{\text{SNR}}{\beta M}\mathbf{G}^H\mathbf{R}^{\text{3D}}_{\text{Rx}}\mathbf{G}\mathbf{R}^{\text{3D}}_{\text{Tx}}\right)\right\}. \tag{30}$$

From [5, (29)], 3D SC can be further decomposed as

$$\mathbf{R}^{\text{3D}}_{\text{Rx}} \approx \mathbf{R}^{\text{2D}}_{\text{Rx}}\odot\mathbf{R}^{\text{el}}_{\text{Rx}},\ \mathbf{R}^{\text{3D}}_{\text{Tx}} \approx \mathbf{R}^{\text{2D}}_{\text{Tx}}\odot\mathbf{R}^{\text{el}}_{\text{Tx}}, \tag{31}$$

where $\mathbf{R}^{\text{el}}_{\text{Rx}}$ and $\mathbf{R}^{\text{el}}_{\text{Tx}}$ denote the elevation SC matrix at the Rx and Tx, respectively.

This article has been accepted for publication in a future issue of this journal, but has not been fully edited. Content may change prior to final publication. Citation information: DOI 10.1109/LCOMM.2017.2765307, IEEE Communications Letters

$$R_{mm'}^{\text{3D,Num}} = \int_\theta \left(\int_{-\pi}^{\pi} A_{\text{H}}(\phi) e^{-j2\pi(d_x \sin\theta\cos\phi + d_y \sin\theta \sin\phi)} \frac{1}{2\pi} d\phi \right) A_{\text{V}}(\theta) f(\theta) e^{-j2\pi d_z \cos\theta} d\theta \tag{18}$$

$$= \int_\theta \left(\int_{-\pi}^{\pi} \sum_{n=0}^{N} a_n \cos(n\phi) e^{-j2\pi d_{xy} \sin\theta\cos(\phi-\Delta)} \frac{1}{2\pi} d\phi \right) c_\kappa A_{\text{V}}(\theta) f_1(\theta) e^{-j2\pi d_z \cos\theta} d\theta \tag{19}$$

$$= \sum_{n=0}^{N} a_n c_\kappa \int_\theta \left(\int_{-\pi}^{\pi} \cos(n(\phi-\Delta)) \cos(n\Delta) e^{-j2\pi d_{xy} \sin\theta\cos(\phi-\Delta)} \frac{1}{2\pi} d\phi + 0 \right) A_{\text{V}}(\theta) f_1(\theta) e^{-j2\pi d_z \cos\theta} d\theta \tag{20}$$

$$= \sum_{n=0}^{N} a_n (-j)^n \cos(n\Delta) c_\kappa \int_0^{\pi} J_n(2\pi d_{xy} \sin\theta) A_{\text{V}}(\theta) f_1(\theta) e^{-j2\pi d_z \cos\theta} d\theta \tag{21}$$

$$= \sum_{n=0}^{N} a_n (-j)^n \cos(n\Delta) c_\kappa \int_0^{\pi} J_n(2\pi d_{xy} \sin\theta) A_{\text{V}}(\theta) f_1(\theta) \left(J_0(-2\pi dz) + 2\sum_{r=1}^{R} j^r J_r(-2\pi d_z) \cos(r\theta) \right) d\theta. \tag{22}$$

$$R_{mm'}^{\text{3D,Num}} \approx \sum_{n=0}^{N} a_n (-j)^n \cos(n\Delta) c_\kappa \int_0^{\pi} J_n(2\pi d_{xy} \sin\theta) \sum_{l=0}^{L} k_l \cos(2l\theta) \left(J_0(-2\pi dz) + 2\sum_{r=1}^{R} j^r J_r(-2\pi d_z) \cos(r\theta) \right) d\theta \tag{24}$$

$$= \sum_{n=0}^{N} a_n (-j)^n \cos(n\Delta) c_\kappa \sum_{l=0}^{L} k_l \left[J_0(-2\pi dz) \int_0^{\pi} J_n(2\pi d_{xy} \sin\theta) \cos(2l\theta) d\theta + \sum_{r=1}^{R} j^r J_r(-2\pi d_z) \right.$$
$$\left. \int_0^{\pi} J_n(2\pi d_{xy} \sin\theta) \left(\cos((r-2l)\theta) + \cos((r+2l)\theta) \right) \right] d\theta \tag{25}$$

$$= \sum_{n=0}^{N} a_n (-j)^n \cos(n\Delta) c_\kappa \left\{ \sum_{l=0}^{L} k_l \pi \left[J_0(-2\pi d_z) J_{\frac{n}{2}-l}(\pi d_{xy}) J_{\frac{n}{2}+l}(\pi d_{xy}) + \sum_{r=1}^{R} j^r J_r(-2\pi d_z) \right.\right.$$
$$\left.\left. \left(\cos(N_{1r}\pi) J_{\frac{n}{2}-N_{1r}}(\pi d_{xy}) J_{\frac{n}{2}+N_{1r}}(\pi d_{xy}) + \cos(N_{2r}\pi) J_{\frac{n}{2}-N_{2r}}(\pi d_{xy}) J_{\frac{n}{2}+N_{2r}}(\pi d_{xy}) \right) \right] \right\}. \tag{26}$$

As lower SC between antenna elements will lead to higher channel capacity, SC matrix with all non-diagonal values being the maximum (or minimum) value will lead to the lower (or upper) bound on channel capacity. For example, defining the bounding elevation SC matrix $\mathbf{R}_{\text{Rx}}^{\text{el,B}}$ and $\mathbf{R}_{\text{Tx}}^{\text{el,B}}$ which satisfy

$$[\mathbf{R}_{\text{Rx}}^{\text{el,B}}]_{ij} = \rho, \ [\mathbf{R}_{\text{Tx}}^{\text{el,B}}]_{pq} = \rho, \ (i \neq j, p \neq q), \tag{32}$$

where $\rho =$ *max* (or *min*) $\left\{ \left| [\mathbf{R}_{\text{Rx}}^{\text{el}}]_{ij} \right|, \left| [\mathbf{R}_{\text{Tx}}^{\text{el}}]_{pq} \right|, (i \neq j, p \neq q) \right\}$. Then, rewrite $\mathbf{R}_{\text{Rx}}^{\text{el,B}}$ and $\mathbf{R}_{\text{Tx}}^{\text{el,B}}$ as

$$\mathbf{R}_{\text{Rx}}^{\text{el,B}} = \rho \mathbf{E}_{\text{Rx}} + (1-\rho)\mathbf{I}_{\text{Rx}}, \ \mathbf{R}_{\text{Tx}}^{\text{el,B}} = \rho \mathbf{E}_{\text{Tx}} + (1-\rho)\mathbf{I}_{\text{Tx}}, \tag{33}$$

where $\mathbf{E}_{\text{Rx}}$ and $\mathbf{E}_{\text{Tx}}$ denote the matrix with all elements being 1 in a dimension of $Q \times Q$ and $M \times M$, respectively. Thirdly, substituting (33) into (31), the bounding SC matrix $\mathbf{R}_{\text{Rx}}^{\text{3D,B}}$ and $\mathbf{R}_{\text{Tx}}^{\text{3D,B}}$ are calculated as

$$\mathbf{R}_{\text{Rx}}^{\text{3D,B}} = \mathbf{R}_{\text{Rx}}^{\text{2D}} \odot \mathbf{R}_{\text{Rx}}^{\text{el,B}} = \rho \mathbf{R}_{\text{Rx}}^{\text{2D}} + (1-\rho)\mathbf{I}_{\text{Rx}}, \tag{34}$$

$$\mathbf{R}_{\text{Tx}}^{\text{3D,B}} = \mathbf{R}_{\text{Tx}}^{\text{2D}} \odot \mathbf{R}_{\text{Tx}}^{\text{el,B}} = \rho \mathbf{R}_{\text{Tx}}^{\text{2D}} + (1-\rho)\mathbf{I}_{\text{Tx}}. \tag{35}$$

Finally, substituting (34) and (35) into (30), further simplifications will give the desired bounding capacity $C_{\text{3D}}^{B}(\rho)$ in (16).

C. Proof of Lemma 3

A larger non-diagonal value of SC matrix, ρ in (32), will lead to a smaller channel capacity. When $\rho = 1$ and 0, we obtain the loose lower bound C_{2D} and upper bound $C_{\text{i.i.d}}$, respectively. Under small EAS case, $[\mathbf{R}_{\text{Rx}}^{\text{el}}]_{ij} = 1 - 2\pi^2 d_{z,ij}^2 \varepsilon^2/3$, $[\mathbf{R}_{\text{Tx}}^{\text{el}}]_{pq} = 1 - 2\pi^2 d_{z,pq}^2 \varepsilon^2/3$ (from [5, Lemma 1]), where $d_{z,ij}$, $d_{z,pq}$ denote the vertical spacing between the i^{th} and j^{th} Rx element, the p^{th} and q^{th} Tx element, respectively. Thus the maximum and minimum value of ρ in (32), ρ_0 and ρ_1, can be obtained by picking the minimum and maximum vertical spacing from $\{d_{z,ij}, d_{z,pq}, (i \neq j, p \neq q)\}$, respectively. When $\rho = \rho_0$, we get the tight lower bound C_{3D}^{low}. When $\rho = \rho_1$, we get the tight upper bound C_{3D}^{up}.

REFERENCES

[1] ITU-R, "Framework and overall objectives of the future development of IMT for 2020 and beyond," *San Diego, USA*, 10-18 June 2015.

[2] J. Zhang, Y. Zhang, Y. Yu, R. Xu, Q. Zheng, and P. Zhang, "3D MIMO: How much does it meet our expectations observed from massive channel measurements?" *IEEE Journal on Selected Areas in Communications*, vol. 35, no. 8, pp. 1887-1903, 2017.

[3] A. Kammoun, H. Khanfir, Z. Altman, M. Debbah, and M. Kamoun, "Preliminary results on 3D channel modeling: From theory to standardization," *IEEE Journal on Selected Areas in Communications*, vol. 32, no. 6, pp. 1219–1229, 2014.

[4] Y. Yu, J. Zhang, and M. Shafi, "3D vs. 2D channel capacity of outdoor to indoor scenarios derived from measurements in China and New Zealand," in *2016 24th European Signal Processing Conference (EUSIPCO 2016)*, Aug 2016, pp. 1980–1984.

[5] Y. Yu, P. J. Smith, P. A. Dmochowski, J. Zhang, and M. Shafi, "3D vs. 2D channel models: Spatial correlation and channel capacity comparison and analysis," in *2017 IEEE International Conference on Communications (ICC)*. IEEE, 2017, pp. 1–7.

[6] S. K. Yong and J. S. Thompson, "Three-dimensional spatial fading correlation models for compact MIMO receivers," *IEEE Transactions on Wireless Communications*, vol. 4, no. 6, pp. 2856–2869, 2005.

[7] K. Rosengren and P.-S. Kildal, "Radiation efficiency, correlation, diversity gain and capacity of a six-monopole antenna array for a MIMO system: theory, simulation and measurement in reverberation chamber," *IEE Proceedings-Microwaves, Antennas and Propagation*, vol. 152, no. 1, pp. 7–16, 2005.

[8] A. Kammoun, M. Debbah, M.-S. Alouini *et al.*, "A generalized spatial correlation model for 3D MIMO channels based on the Fourier coefficients of power spectrums," *IEEE Transactions on Signal Processing*, vol. 63, no. 14, pp. 3671–3686, 2015.

[9] 3GPP TR 36.873 V.2, "Study on 3D channel model for LTE (Release 12)," Technical Report, 2014.

[10] D. Ying, F. W. Vook, T. A. Thomas, D. J. Love, and A. Ghosh, "Kronecker product correlation model and limited feedback codebook design in a 3D channel model," in *Communications (ICC), 2014 IEEE International Conference on*. IEEE, 2014, pp. 5865–5870.

[11] D. P. Palomar, J. R. Fonollosa, and M. A. Lagunas, "Capacity results of spatially correlated frequency-selective MIMO channels in UMTS," in *Vehicular Technology Conference, 2001. VTC 2001 Fall. IEEE VTS 54th*, vol. 2. IEEE, 2001, pp. 553–557.

[12] I. S. Gradshteyn and I. M. Ryzhik, *Table of Integrals, Series, and Products (seventh edition)*. Academic Press, 2014.

[13] D. A. Harville, *Matrix algebra from a statistician's perspective*. Springer, 1997, vol. 1.